ARTICLE

ω-Unsaturated methacrylate macromonomers as reactive polymeric stabilizers in mini-emulsion polymerization

Received 00th January 20xx,
Accepted 00th January 20xx

DOI: 10.1039/x0xx00000x

Joshua R. Booth,[a] Joshua D. Davies,[a] and Stefan A. F. Bon*[a]

Polymer latexes of poly(benzyl methacrylate) P(BzMA) were synthesized by mini-emulsion polymerization, using hexadecane as the hydrophobe and ω-unsaturated methacrylate-based macromonomers as a reactive stabilizer. The amphiphilic macromonomers were synthesized by catalytic chain transfer emulsion polymerization (CCTP) and subsequent chain extension via sulfur-free reversible addition-fragmentation chain transfer (SF-RAFT). Their critical micelle concentration (CMC) was determined by dynamic light scattering (DLS), and micelle size was measured using DLS and small angle x-ray scattering (SAXS). The surface activity of the stabilizers was measured by pendant drop tensiometry and compared to modelled behaviour. For the mini-emulsion polymerizations, macromonomer stabilizers were added at a range of concentrations, with respect to the dispersed phase. Using less than 5 wt% stabilizer, SEM micrographs showed many of the particles were bowl-shaped. This morphology was studied in depth and we propose that monomer transport occurs between particles during polymerization towards the smaller particles as a direct result of compartmentalization. At concentrations of 5 wt% and higher, bimodal droplet and particle distributions were observed by DLS and SEM. We propose shear-dependent depletion flocculation as the explanation. Lastly, the effectiveness of the reactive stabilizers was tested in terms of latex stability and molecular weight control. Resistance to coagulation during freeze-thaw cycles and prolonged dialysis were tested. Examination of P(BzMA) reaction kinetics and molecular weight indicated that the incorporation of macromonomer is gradual and less than quantitative at the end of the polymerization process, in agreement with the mechanistic understanding.

Introduction

Polymeric stabilizers are interesting to use in the synthesis of polymer colloids by heterogeneous polymerization techniques, such as emulsion and mini-emulsion polymerization. They can serve as particle nucleation sites. They lower the interfacial tension at the colloid-liquid interface and they improve colloidal stability of the colloidal dispersions by steric and/or electrostatic means. One can argue that molecular surfactants of low molar mass can do the same, but their polymeric counterparts come with some added advantages. To think of an obvious benefit, polymeric stabilizers generally adhere stronger to the surface of polymer colloids. This limits or even prevents surfactant migration upon product formulation, which if occurs, can cause foaming and destabilization. Surfactant migration in the end application is also problematic. Examples include uptake of water and thus whitening of clear polymer films, or allergic reactions to small organic surfactants in dipped goods, such as gloves.

Department of Chemistry, University of Warwick, Coventry, CV4 7AL, United Kingdom https://www.bonlab.info/
*Email: s.bon@warwick.ac.uk

Electronic Supplementary Information (ESI) available: Details of reaction recipes, PBzMA surface free energy and SAXS fitting parameters, CCTP reaction scheme, ^{1}H NMR spectra for P(MAA-*co*-MMA) and P(BMA-*b*-[MAA-*co*-MMA]) macromonomers, droplet size during homogenization, high magnification SEM micrographs, additional particle characterization and molecular weight distributions

Generally, when referring to polymeric stabilizers, we mean amphiphilic macromolecules. Their use in emulsion polymerization has been well documented,[1–4] with mini-emulsion polymerization receiving less attention.[5]

Mini-emulsion polymerization can be seen as a variation of a conventional emulsion polymerization process. The key difference is that the polymerization reaction proceeds *via* droplet nucleation as the main process of particle formation, instead of homogeneous and/or micellar nucleation. To realize this, the diameter of the monomer droplets in a mini-emulsion are reduced to submicron dimensions, in the range of say 40-800 nm. This can be done using high energy emulsification techniques, such as ultrasonication or high-pressure homogenization. This decrease in diameter, d, of the mini-emulsion droplets increases the overall droplets' surface area substantially, as the area-to-volume ratio equals $6d^{-1}$. When using a water-soluble initiator, as in emulsion polymerization, this increases the probability for radical entry into the monomer droplets greatly. The average chain-length of radical species that undergo entry in mini-emulsion polymerization remains under debate.

Since its conceptualization in the 1970s,[6] water-based mini-emulsion polymerization has emerged as a versatile technique, enabling the heterogeneous polymerization of highly water-insoluble monomers,[7,8] as well as the encapsulation of inorganic particles[9–11] and hydrophobic liquids.[12,13] These feats are made possible since mini-emulsion droplets formed by high energy

emulsification are said to be 'critically stabilised' against two processes, Ostwald ripening and coalescence.[14] The first is a thermodynamically driven process, a direct result of a difference in Laplace pressure, in which smaller droplets shrink in favour of larger ones by monomer diffusion through the continuous phase.[15,16] The second occurs when colliding droplets overcome forces of repulsion and fuse. The key to the success of the mini-emulsion polymerization process is that Ostwald ripening can be suppressed by using a low molecular weight ultra-hydrophobic compound, knowns as a hydrophobe or co-stabilizer, increasing the mini-emulsion stability from seconds/hours to days/months.[17] The reason is an osmotic pull-back (swelling capacity) countering the drive for Ostwald ripening. Droplet coalescence is prevented with the use of surfactants. During the emulsification process a steady-state is reached where the amount of surfactant partitions between phases and the interface of the droplets. Typical mini-emulsions have less than 100% surface coverage, which is logical to promote droplet nucleation as the sole nucleation mechanism.[18]

As said before, polymeric stabilizers exhibit significant differences from small-molecule surfactants. This has consequences on the mini-emulsion polymerization process and final polymer latex. Their lower rate of droplet desorption and slower diffusivity can lessen the chance of secondary nucleation and retard Ostwald ripening.[19–21] Rather than adhering to the surface of the droplets/particles solely by physisorption, polymeric surfactants are easily grafted covalently upon mini-emulsion polymerization through radical chain transfer events. This further prevents desorption from particle surfaces upon dilution, dialysis, or formulation. Grafted stabilisers that form dense surface layers can also prevent particle coalescence during freezing-thaw cycles of the polymer latex.[22]

A variety of polymeric stabilizers have been employed in mini-emulsion formulations, including anionic alkyl soluble resins,[23–27] cationic statistical[20] and cationic block copolymers,[28,29] as well as non-ionic copolymers.[30–33] An interesting development in the 1980-1990s was the use of reactive surfactants, given names such as surfmers (surfactant-monomer), inisurfs (surfactant-initiator), and transurfs (surfactant – chain transfer agent).[34] Along this theme reactive polymeric stabilizers were developed. The emergence of reversible deactivation radical polymerization (RDRP) allowed for easy design access to a wide variety of reactive polymeric stabilizers. One RDRP technique is reversible addition-fragmentation chain transfer (RAFT) polymerization.

The origin of RAFT polymerization is commonly attributed to work published and patented in the mid to late 1990s, with the use of sulfur-based RAFT agents, such as thiocarbonylthio species.[35–37] However, work by Moad and co-workers that predates this demonstrates that methacrylate-based ω-unsaturated macromonomers (MM), can be used in the same fashion (hint: replace the sulfur atoms in a trithiocarbonate RAFT agent with carbon to see the analogy).[38,39] The activity of these RAFT agents can be rationalised by their chain transfer constants ($C_s = k_{tr}/k_p$), where k_{tr} and k_p are effective rate coefficients for chain transfer and propagation. The popularity of sulfur-based RAFT agents is partially attributed to the much higher reactivity of the C=S bond than the MM C=C bond. The methacrylate-based MMs have a much lower chain transfer constant than typical thiocarbonylthio species, that is ≈ 0.3 *vs* >100.[40,41] The acronym AFCT, addition-fragmentation-chain-transfer, is also used for these less reactive systems.

The use of sulfur-based RAFT agents that doubled as mini-emulsion stabilizers were first reported in 2003 by Hawkett and co-workers,[42] who investigated the use of poly(acrylic acid)$_5$–*block*-poly(*n*-butyl acrylate)$_{20}$ and poly(acrylic acid)$_5$-*block*-poly(styrene)$_{20}$ macroRAFT agents. In 2010, Hawkett and co-workers expanded on their findings by analysing the influence on particle size and number and molecular weight control of four P(AA-*b*-Sty) macroRAFT agents.[21] Luo and co-workers investigated the influence of macroRAFT agent aqueous phase solubility on secondary nucleation and molecular weight control.[43,44] They also studied the effect of SDS and the degree of ionization of P(AA$_{16}$-*co*-Sty$_7$) macroRAFT agents on particle and molecular weight distributions.[45,46] As well as carboxylic acid functionalised stabilizers, RAFT agents containing polyethylene oxide (PEO) either in the polymer backbone or as sidechains have also been used to control particle size and molecular weight. D'Agosto *et al.* used PEO based RAFT agents with dithiobenzoate, thiopropyl or thiododecyl z-groups.[47] Due to the reduction in aqueous phase RAFT agent concentration, it was found PEO based thiopropyl RAFT agent gave the best control of particle size and molecular weight. Cheng *et al.* modified PEO$_{45}$-*b*-PSty RAFT agents with norbornene and grafted multiple chains together via ring-opening metathesis polymerization.[48] Both precursor and grafted RAFT agents were effective stabilizers but lead to capsule formation when crosslinking monomer was added. Similar particle morphologies were also reported by Rieger and co-workers with poly(acrylic acid-*co*-poly[ethylene oxide] acrylate) RAFT agents.[49]

The use of ω-unsaturated methacrylate-based macromonomers as stabilizers in heterogeneous polymerizations, as alternative to sulfur-based RAFT agents, is of renewed interest. They are easily accessible by catalytic chain transfer polymerization (CCTP), mediated by Cobalt(II)-species.[50] The use of these MMs in emulsion polymerization has been reported. For example, water-soluble MAA MMs were used independently by Heuts and Haddleton to produce stabilizers *in-situ*.[51,52] A drawback is the loss of control of polymer chain growth which leads to an uncontrollable increase in the kinetic chain length and thus polymer molecular weight.[53] On self-assembly of the amphiphilic MMs into primary latex particles or upon their entry into pre-existing particles, the local monomer concentration increase and shifts the balance of control, as now $k_p[M] > k_{tr}[MM]$. However, this can be solved by using 'pre-formed' amphiphilic thermoresponsive MMs, clearing the path for polymerization induced self-assembly (PISA).[54] Ex-situ formed amphiphilic MMs were used in emulsion polymerization by Chen and co-workers but all successful reactions required additional small-molecule surfactant.[55] Stable latexes were produced by Heuts and co-

workers using only P(MAA-*b*-MMA) or P(BA-*b*-MAA) macromonomers[56] as well as statistical copolymer MMs.[57] Beside emulsion polymerization, it is noteworthy to mention that Hutchinson reported the use of MMs as stabilizers in semi-batch non-aqueous dispersion polymerizations.[58,59]

To reduce the use of volatile organic solvents and time spent on polymer solution work-up, amphiphilic MM can be synthesized by emulsion polymerization. In our previous work we demonstrated the effectiveness of (P(BMA-*b*-[MAA-*co*-MMA]) MMs in the stabilisation of high solids PBMA latexes.[60] The influence of pH before and during the reaction was also investigated by Haddleton and co-workers.[61] Going a step beyond, MM micelles were also covalently crosslinked and used as nanogel stabilizers.[62,63] To the best of our knowledge the use of MMs as reactive stabilizers in water-based mini-emulsion polymerization has received little attention. This is what this study is about.

Herein, poly(*n*-butyl methacrylate-*block*-[methacrylic acid-*co*-methyl methacrylate]) (P(BMA-*b*-[MAA-*co*-MMA]) macromonomer latexes were synthesized in a two-stage emulsion polymerization process. This heterogeneous synthesis route avoids the use of volatile organic solvents, which is highly preferable for industrial applications. Furthermore, the pH-dependant disassembly of MM latex particles into an aqueous dispersion of micelles completely negates the time-consuming work-up of MM solutions in organic solvents. The block copolymer stabilizers are versatile, with the ability to alter the block type and length like typical RAFT agents but without the malodour and colour originating from the thiocarbonylthio group. In this study, the particle size distribution and surface activity characterization of the MM micelles is discussed before being used as the sole stabilizer in the mini-emulsion polymerization of benzyl methacrylate (BzMA). This monomer was chosen to avoid the substantial auto-acceleration (Trommsdorff-Norrish) effect associated with monomers such as MMA,[64,65] which would have complicated molecular weight analyses. Particle size distributions of the resulting latexes together with particle morphology is investigated. The colloidal stability of the particles was assessed and the reaction kinetics were briefly examined.

Experimental

Materials

n-Butyl methacrylate (BMA, 99%), benzyl methacrylate (BzMA, 96%), methacrylic acid (MAA, 99%), methyl methacrylate (MMA, 99%), potassium persulfate (KPS, 99%), sodium dodecyl sulfate (SDS, ≥99.0%) and (trimethylsilyl)diazomethane solution (2M in hexanes) were purchased from Sigma-Aldrich. 4,4'-Azobis(4-cyanovaleric acid) (ACVA, 75%), *n*-hexadecane (HD, ≥99%) were purchased from Alfa Aesar. 2,2'-Azobis(2-methylpropionitrile) (AIBN), purchased from Alfa Aesar, was recrystallised from methanol and stored at -5 °C. Bis[(difluoroboryl)diethylglyoximato]cobalt(II) (CoEtBF) was synthesized using an analogous procedure described for CoBF.[66] Deionized water (≥15 MΩ) was used throughout.

Synthesis of poly(*n*-butyl methacrylate-*block*-[methacrylic acid-*co*-methyl methacrylate]) colloidal dispersion by emulsion CCTP and seeded RAFT polymerization

Block copolymer macromonomer (MM) aqueous dispersions were prepared following our previously published procedure[60] adapted from work by Krstina *et al.*,[39] Moad *et al.*[40] *and* Suddaby *et al*.[67]Poly(methacrylic acid-*co*-methyl methacrylate) macromonomers were synthesised using reagents in Table 1. This macromonomer latex was used in the synthesis of particles of poly(*n*-butyl methacrylate-*block*-[methacrylic acid-*co*-methyl methacrylate]) macromonomers using the ingredients listed in Table 2. To produce an aqueous dispersion of polymeric stabilizers, ammonium hydroxide 35% w/w (8.527 g, 5% mol excess to MAA units) was added to the P(BMA-*b*-[MAA-*co*-MMA]) latex (500 g) and diluted with water (230 g). The latex was heated to 70 °C for 30 mins, changing to a transparent, viscous liquid.

Table 1 Recipe for the synthesis of poly(methacrylic acid-*co*-methyl methacrylate) latex

Ingredient	Quantity
MMA	52.64 g (56 mL, 0.52 mol)
MAA	24.48 g (24 mL, 0.28 mol)
CoEtBF	4.693 mg (1.05×10^{-5} mol)[a]
SDS	1.2 g
ACVA	2.0 g (7.14 mmol)
Water	520.0 g

[a]Molar ratio of monomer:CoEtBF = 76959:1

Table 2 Recipe for the synthesis of poly(*n*-butyl methacrylate-*block*-[methacrylic acid-*co*-methyl methacrylate]) latex

Ingredient	Quantity
MM latex	500.0 g (MM 65.6 g, 10.7 mmol)
nBMA	49.0 g (54.8 mL, 344.6 mmol)
KPS	0.3069 g (1.13 mmol)
Water	214.0 g

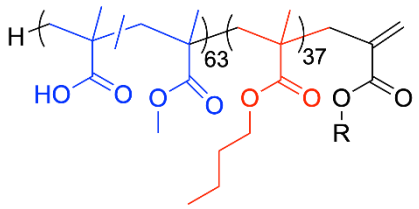

Scheme 1 Chemical formula of poly(*n*-butyl methacrylate-*block*-[methacrylic acid-*co*-methyl methacrylate]) macromonomer stabilizer. The hydrophilic and hydrophobic blocks have been coloured blue and red, respectively.

Batch mini-emulsion polymerization of benzyl methacrylate in presence of macromonomer stabilizers

An aqueous phase was prepared by adding the concentrated aqueous MM dispersion (10.14% wt/wt, 1.25, 2.5, 5, 7.5 and 10 wt% MM w.r.t dispersed phase) to water (total water mass 32.0 g). To the aqueous phase, a premixed dispersed phase of BzMA (7.6 g, 43.13 mmol), HD (0.4 g, 1.77 mmol) and AIBN

Table 3 Characterization of poly(*n*-butyl methacrylate-*block*-[methacrylic acid-*co*-methyl methacrylate]) macromonomer. Number average molcular weight values were calculated by ^{1}H NMR (a) and SEC (b).

Macromonomer molecular weight							Size and aggregation				
$M_{n,NMR}$[a]/ g mol^{-1}	DP_n/ -	DP_{BMA}/ -	$DP_{MAA\text{-}b\text{-}MMA}$	M_n[b]/ g mol^{-1}	M_w/ g mol^{-1}	Đ/ -	R_{theory}/ nm	R_H/ nm	R_{SAXS}/ nm	CMC/ g L^{-1}	CMC/ M × 10^6
11300	101	37	64	10800	18800	1.74	20.1	32.0	13.3	0.021	1.9

(0.01 g, 6.09 x 10^{-2} mmol) was added and stirred for 30 minutes with a magnetic stirrer. The mixture was then dispersed with an IKA ULTRA-TURRAX rotor-stator homogenizer for 2 minutes at 12,000 rpm. The emulsion was immediately transferred into an Avestin Emulsiflex C3 high-pressure homogenizer. It was processed 20 times, with each pass using a homogenizing pressure of 12,500 psi. The mini-emulsion was transferred to a round-bottom flask and purged with nitrogen for 30 mins. After purging, the mini-emulsion was heated to 70 °C and maintained overnight under a positive pressure of nitrogen, with stirring at 300 rpm. Samples were taken for monomer conversion and molecular weight analysis. Experimental reagent quantities are listed in Table S1.

Characterization methods

Densitometry: Density values were measured at 20 °C using a Schmidt Haensch density meter. For block copolymer macromonomer density values, measurements were conducted on a dispersion of concentration 1 g L^{-1}. The density value was taken as the average of 10 individual runs.

Drop shape analysis: Interfacial tension (γ) values were measured at 20 °C on a KRÜSS DSA 100 drop shape analyzer. At the measurement temperature of 20 °C, the densities of *n*–dodecane (DD), water and the block copolymer macromonomer solution (1 g L^{-1}) were 0.750, 0.997 and 0.997 g cm^{-3}, respectively. Measurements were conducted using a J-shape dosing needle of inner diameter 1.120 mm, supplied by C. Gerhardt UK. The dispersed phase was DD and continuous phase was the block copolymer aqueous dispersion. The DD was saturated with water before use and the continuous phase was saturated with DD prior to measurement. Images of the droplet were taken every 10 seconds for 12 hours and the interfacial tension values were calculated using ADVANCE software image analysis via the Young-Laplace equation.

To calculate the surface free energy of poly(benzyl methacrylate) (P(BzMA)) films, sessile drop measurement were used. The interfacial tension values of $\gamma_{PBzMA\text{-}HD}$ and $\gamma_{PBzMA\text{-}Aqu}$ were calculated using the OWRK method and water and ethylene glycol as standards. The contact angles for the MM aqueous phase on P(BzMA) films were measured in triplicate. The contact angle for HD on the film was extremely low and a single measurement was recorded. Contact angles and surface free energy tabulated in Table S2.

Dynamic light scattering (DLS): Size and scattering intensity measurements were conducted on a Malvern Zetasizer Nano ZS particle size analyzer. Measurements were performed at a scattering angle of 173° at 25 °C. For size measurements, mini-emulsion droplets were diluted with water saturated with the emulsified phase and particles were diluted in pure water. To measure the critical micelle concentration (CMC), micelle dispersions were diluted with the appropriate amount of 1 mM $NaHCO_3$ solution, filtered through hydrophilic-PTFE membranes with 0.45 µm pore size and equilibrated at room temperature overnight. The attenuator setting number was fixed during the measurements.

Gas chromatography: Monomer conversion was measured using a Shimadzu GC-2014 system equipped with a Shimadzu A020i autosampler, flame ionisation detector (flame temperature 300 °C, sampling rate of 40 ms) and Restek Rxi1ms column (14.9 m length, 0.25 mm inner diameter and 0.25 µm film thickness). Injection temperature was 200 °C, injection volume 1 µL with split ratio of 60:1. Hydrogen carrier gas column flow rate was 1.19 mL min^{-1}. The heating profile was 45 °C for 1 min, increase to 55 °C at 20 °C min^{-1} and hold for 5 min then increase to 300 °C at 40 °C min^{-1} and hold for 7.5 min. Latex samples were dissolved in THF and filtered through PTFE filter with 0.2 µm pore size. Monomer concentration was determined through comparison of the peak area ratio, monomer/hexadecane, with [HD] assumed to be constant throughout reactions.

Size exclusion chromatography (SEC): Polymer molecular weight analysis was carried out using an Agilent Infinity II MDS instrumentation equipped with differential refractive index, viscometry, dual angle light scatter, and multiple wavelength UV detector. The system was equipped with 2 x PLgel Mixed C columns (300 × 7.5 mm) and a PLgel 5 µm guard column. THF with 0.01% butylated hydroxytoluene additive was used as the eluent. Samples were run at 1 mL min^{-1} at 30 °C. PMMA and PS standards (Agilent EasyVials) were used for calibration. For the analyses of P(MAA-*co*-MMA) and P(BMA-*b*-[MAA-*co*-MMA]) the carboxylic acid groups were esterified to methyl groups using *in situ* generated diazomethane.[68,69]Analyte samples were filtered through a PTFE membrane with 0.2 µm pore size before injection. Experimental molar mass (M_n and M_w) and dispersity (Đ) values of synthesised polymers were determined by conventional calibration against PMMA standards using Agilent GPC/SEC software. The Mark–Houwink (MHKS) parameters used for analysing PMMA samples were K = 14.1x10^{-3} mL g^{-1} and α = 0.70. The MHKS parameter pairs when analysing benzyl methacrylate (PBzMA) samples were K = 12.8x10^{-3} mL g^{-1} and α = 0.690 for PMMA[70] and K = 3.32x10^{-3} mL g^{-1} and α = 0.701 for PBzMA[71].

Nuclear magnetic resonance spectroscopy: ^{1}H NMR experiments were conducted on a Bruker Avance III HD 400 MHz instrument. Chloroform-d and dimethyl sulfoxide-d_6 was

purchased from Sigma-Aldrich. Spectra were analyzed using ACD laboratories software.

Scanning electron microscopy: Samples were imaged on a ZEISS GeminiSEM Field Emission Scanning Electron Microscope. Samples were imaged at an accelerating voltage of 0.2 kV and working distance of 2.0 mm. Latexes were diluted, drop cast onto silicon wafer, dried overnight and coated with a layer of carbon via physical vapor deposition.

Small angle X-ray scattering: Measurements were carried out using a 5m Xenocs Xeuss 2.0 SAXS instrument equipped with dual microfocus (Cu/Mo) sources and a Pilatus 300K hybrid photon counting detector. X-ray wavelength was 1.542 Å. Samples were diluted to 5 mg mL^{-1} with 10 mM NaOH. Glass capillaries containing the samples were mounted in a furnace stage at 30 °C. Scattering patterns were analysed using SasView5 software. Details of fitting parameters used can be found in supporting information (Table S3).

Results and discussion

Characterization of macromonomers

Water-based micellar dispersions of the ω-unsaturated methacrylate-based block copolymer stabilizers were synthesized in three steps. Firstly, poly(methacrylic acid-*co*-methyl methacrylate) (P(MAA-*co*-MMA)) macromonomers (MM) were produced by catalytic chain transfer mediated emulsion polymerization (CCTP), employing a cobalt catalyst (Scheme S1). Owing to the presence of the ω-unsaturated end group on the polymer chains, poly(*n*-butyl methacrylate-*block*-[methacrylic acid-*co*-methyl methacrylate]) (P(BMA-*b*-[MAA-*co*-MMA]) macromonomers were synthesized by sulfur-free reversible addition-fragmentation chain transfer (RAFT) polymerization. The resultant polymer latexes of these two steps are highly processable, no work-up is required and the syntheses are easily scalable (currently operating at 1L scale). Lastly, the block copolymer latex particles were disassembled into a dispersion of polymeric micelles with the addition of base to protonate the carboxylic acid groups. All measurements and further reactions were conducted at pH ≥8.8 to ensure close to full deprotonation.[72–74] This ensured consistent stabilising efficiency, as the aggregation of amphiphilic block copolymers has been shown to be dependent on the degree of ionization of acid groups.[75,76]

The molecular weight of the stabilizers was measured by ^{1}H NMR spectroscopy and size exclusion chromatography (SEC), the results of which are presented in Table 3. A target hydrophobic:hydrophilic block length of 1:2 was chosen to favour a micellar supramolecular morphology.[77,78] The individual average block lengths were calculated by ^{1}H NMR using the integral ratio of ω-end group vinyl protons (5.45 and 6.15 ppm) to protons in the polymer backbone, or side group. For the P(MAA-*co*-MMA) block, signals from the methyl and methylene protons in the backbone (0.25-2.25 ppm) were used (Figure S1). For the PnBMA block, the side chain CH_2 protons closest to the ester group (3.90 ppm) were used (Figure S2). The value for M_n calculated by NMR, 11300 g mol^{-1}, is in good agreement with the results obtained from SEC analysis. Note that to improve solubility for SEC analysis the carboxylic acid groups were esterified following a procedure by Lacík *et al.*[68,69] prior to analysis. The similar values indicate that a high number of chains possess an ω-unsaturated group.

Owing to the amphiphilic character of the macromonomers (MM), aggregation of unimers into micelles occurs above a certain concentration in water. The critical micelle concentration was (CMC) studied using DLS, shown in figure 1a. The intensity of scattered light in a DLS measurement is recorded in kilo counts per second (kcps). As the concentration of MM increases, so does the intensity of scattered light. At 0.021 g L^{-1} (1.9×10^{-6} M) [MM] there is a change in gradient at which the kcps value increases. Above this point the excess amount of MM assembles into supramolecular micellar structures that scatter more. This point we refer to as the CMC and its value falls in line with other literature CMC values for amphiphilic block copolymers.[56,80,81]

Following the confirmation of aqueous self-assembly, the size of the aggregates was measured by two orthogonal techniques. Both techniques use scattering of polarised electromagnetic radiation to determine an average size. Aggregate average radii from dynamic light scattering and small angle x-ray scattering techniques are shown in Table 3 alongside an estimate for the theoretical dimensions.

For comparison, it is important to first calculate the approximate theoretical MM micelle radius (R_{theory}). The hydrophilic block (MAA-*co*-MMA) has a DP_n of 65 by NMR. Throughout all of the measurements and reactions, the pH of the aqueous phase is maintained at pH 8.8 to ensure a high degree of ionisation.[72–74] Considering this, the hydrophilic block of the micelle corona may be considered fully extended and is equal to the contour length (L_{max}; see equation 1).[82] Where *n* is the number of C-C bonds and *lcos(θ/2)* is the projected length of the bond with length *l* and angle θ along the contour. The contour length assumes for a backbone consisting of sp^3 hybridized carbons, all bonds are trans configuration with bond angle θ 68 °.

$$L_{max} = n \cdot l \cdot cos\left(\frac{\theta}{2}\right) \quad (1)$$

This results in a value of 16.34 nm for the hydrophilic block length of the MM molecules in the micelles. The BMA blocks of the MMs in a micelle are much more densely packed and can be approximated as ideal chains. This situation is almost never realised but linear polymer melts and concentrated solutions are close to ideal.[82] The mean-square end-to-end length ($\langle R^2 \rangle$) of an idea chain is calculated using equation 2. Where *n* and *l* are the number and length of the chain bonds and C_∞ is characteristic ratio determined by Flory.[83]

$$\langle R^2 \rangle = C_\infty n l^2 \quad (2)$$

For PBMA, C_∞ is determined as 7.9-8.5.[84,85] Since C_∞ decreases below a critical chain length, 7.9 was used as an approximate value to calculate the length of the BMA block as an ideal chain. Equation 2 for a BMA block of DP_n 37, gives an end-to-end radius of 3.7 nm, however it should be noted this

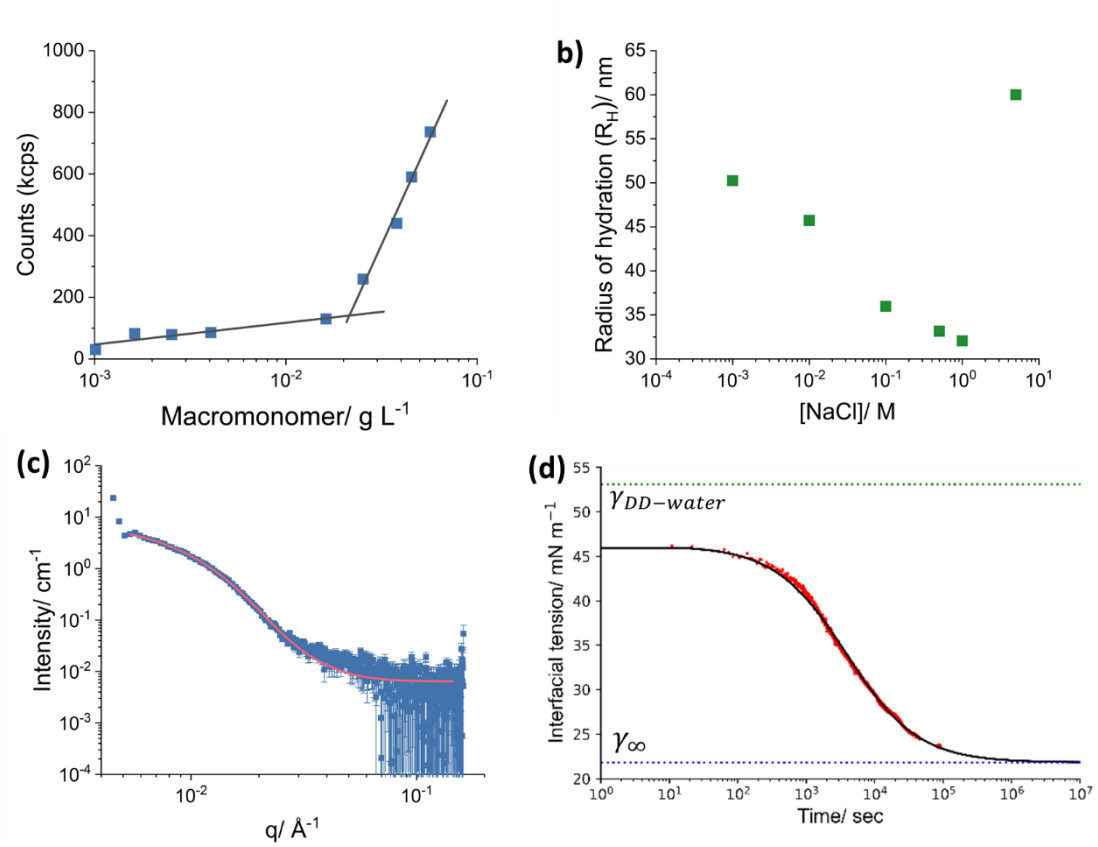

Figure 1 (a) Plot of intensity of scattered light measured by DLS, as a function of macromonomer concentration. Linear fits of two regions are shown in black. The CMC was determined at the intersection point of the linear fits. (b) Micelle hydrodynamic radius, measured by DLS, as a function of salt concentration at 25 °C. (c) SAXS spectra of macromonomer micelles (5 mg mL^{-1} in 10 mM NaOH) measured at 30 °C. The fit, shown in pink, was obtained using sphere form model and RMSA structure factor. (d) Plot showing the change in interfacial tension (IFT) of dodecane in a continuous phase of macromonomer aqueous dispersion (1 g L^{-1}) at 20 °C as a function of time. Experimental data points shown in red and theoretical values shown as the black line. The data fit using the empirical model proposed by Rosen and Hua.[86] The green dotted line represents DD-water IFT at 20 °C ($\gamma_{DD\text{-}water}$), the blue dotted line represents the equilibrium IFT (γ_{∞}).

length is a Gaussian distribution of all possible conformations. Combing the two lengths estimates the overall micelle radius to be 20.1 nm.

The mean hydrodynamic radius (R_H) of the micelles in salt solution was determined by DLS (Table 3, Figure 1b). It should be noted that the size of colloids measured by DLS is influenced by the thickness of a diffuse layer of ions known as the electric double layer (EDL). The effect of NaCl in compressing this layer lowers R_H. The effect of this can be seen in Figure 1b with the lowest R_H recorded to be 32.0 nm at 1M NaCl. Compared to low-molecular weight surfactants a micelle radius of 32 nm seems considerably large. However, for amphiphilic polymeric stabilisers, such sizes are commonplace. For instance, Mohanty and co-workers report R_H of 47.5 nm for poly(styrene$_{90}$-*b*-styrene sulfonate$_{65}$)[86] and Théodoly and co-workers measure the R_H of P(BA$_{23}$-*b*-AA$_{166}$) to be 51 nm, dropping to 30 nm at 1 M NaCl.[87] Although the total block lengths of these polymers are greater than the MM used in this chapter, they were synthesised to much narrower dispersities. Cunningham and co-workers studied the effect of the dispersity of the hydrophobic block or the hydrophilic block of stabiliser performance.[88,89] DLS data shows R_H is sensitive to molar mass dispersity of the chains in both the core and corona. For P(S$_{29}$-b-AA$_{41}$) copolymers, using the same PS block but increasing the dispersity of the AA block, so that the total dispersity increased from 1.13 to 1.54 lead to a two-fold increase in R_H. Given that the dispersity of the MM in this chapter is 1.74, it is likely that the longer chains in the distribution raise the average R_H measured by DLS.

For comparison, the micelle radius was measured by small angle x-ray scattering (SAXS). The scattering data was fitted with a spherical form factor[90] including the Hayter-Penfold Rescaled Mean Spherical Approximation (RMSA) structure factor[91,92] to account for the Coulombic repulsion between charged objects. From the fit shown in Figure 1c, a volume-weighted radius of 13.1 nm was calculated. A core-shell form factor[90] was also used but resulted in a similar total radius. The SAXS measurement appears to underestimate the micelle radius. This is likely due to the lower electron density of the solvated shell causing less scattering of the beam, with the effect being worst the furthest away from the core.

To measure the effectiveness of the macromonomers as stabilizers, their influence of the interfacial tension (IFT, γ) of *n*-dodecane (DD) was measured by drop shape analysis (DSA). The interfacial tension of pure DD measured at 20 °C was 53.12 mN m^{-1}, in good agreement with literature (52.81-52.90 mN m^{-1}).[93–95] Plotting IFT vs time in Figure 1d, the initial IFT value of 46.65 mN m^{-1}, is significantly lower than DD in pure water. This instantaneous drop in IFT can be attributed to the rapid adsorption of macromonomer molecules to the dodecane drop as it is generated from the needle and introduced into the surrounding macromonomer dispersion. The interfacial tension

data points were fit using the empirical model proposed by Rosen and Hua (Figure 1d, black line):[96]

$$\gamma_t - \gamma_\infty = \frac{\gamma_0 - \gamma_\infty}{1 + \left(\frac{t}{t^*}\right)^n} \quad (3)$$

where γ_t is the DD IFT at time t. A three-parameter fit of the data using equation 3 yields values for the equilibrium IFT, γ_∞, of 21.82 mN m^{-1} and two system-specific parameters, n and t^* of 0.83, and 3874.42 s, respectively. It can be seen from Figure 1d that the experimentally obtained IFT data is in good agreement with the model. The Rosen-Hua model predicts, that for the data reported, an equilibrium IFT, γ_∞, of 21.82 mN m^{-1} would be achieved after approximately 280 hours.

Compared to low molecular weight surfactants and other polymeric stabilizers, the decrease in DD IFT is due to the low CMC and high degree of ionization of the P(BMA-*b*-[MAA-*co*-MMA]) macromonomers. The DD droplet, once dispersed in water will have a negative surface potential by itself. Therefore, it is less likely for MM micelles (fully surrounded by a hydrophilic negatively charged layer) to absorb directly. MM unimer adsorption from the bulk phase, is more plausible. The rate of this process is limited by the relatively slow micelle-to-unimer exchange, and the low value of the CMC. Indicatively, Théodoly and co-workers have shown that the kinetics of droplet adsorption of P(BA-*b*-AA) stabilisers are controlled by unimer extraction from micelles.[97] Once unimers begin to build up at the surface there is also a reduction in the rate of adsorption due the steric hindrance from the surface layer.[98] It is also likely that unimer exchange occurs during the measurement as there is greater entropic gain for high molecular weight macromonomers to replace shorter chains.[99,100] Although the kinetics of MM adsorption are slow, this is not an issue when stabilizing mini-emulsion droplets, due to the high shear forces that redistribute the macromonomers during emulsification. In addition, the "ideal" mini-emulsion polymerization process is the conversion of these droplets into particles and, hence, no MM transport or re-partitioning is required.

Mini-emulsions of benzyl methacrylate and hexadecane (5 % w/w) as the dispersed phase and water containing macromonomer stabilizers as aqueous phase were produced by forming a coarse emulsion using a rotor-stator homogenizer followed by a high-pressure homogenizer (HPH). Note that the coarse emulsions coalesced quickly and had to be processed in the HPH immediately after forming. This coalescence can be explained by Stokes' Law in which the terminal velocity of droplets (rate of creaming) increases in larger droplets.[101] The Avestin C5 HPH uses a homogenizing valve (radial diffuser) in which the coarse emulsion experiences elongational flow (shear forces) and turbulence to break droplets into a nanosized dispersion.[102] If the droplets have an uneven distribution of stabilizer they may coalesce to reach an equilibrium size.[103] Due to the irregular nature of this process, multiple passes of the emulsion through the HPH were required to reach a plateau in diameter, as shown in Figure S3. An oil-soluble initiator was use in this series to discourage secondary nucleation.

We will first discuss the morphology of the polymer latex particles after mini-emulsion polymerization. Then, we will make some comments on mechanistic events of the polymerization process.

Mini-emulsion polymerization: dimpled particles

The droplet size before polymerization and final latex particle size was measured by DLS and latexes at full monomer conversion were imaged by scanning electron microscopy (SEM) (figure 2). Studying the SEM micrographs of MM1.25% and MM2.5% (figure 2, right column), spherical recesses or dimples can be seen on many particles. This morphology can also be seen when imaged by transmission electron microscopy (Figure 3a). During mini-emulsion polymerization, the monomer and hexadecane are miscible but the polymer and hexadecane are not. Depending on the interfacial tensions between the polymer, hexadecane and aqueous phase, at full monomer conversion, the hexadecane can be either fully encapsulated, partial encapsulated or totally dissociated.[12,104,105] The morphology for PBzMA, HD and aqueous phase containing MM was predicted using Surface Evolver modelling software and a script published by Brakke.[106,107] The interfacial tensions used for the three phases, $\gamma_{PBzMA\text{-}HD}$, $\gamma_{PBzMA\text{-}Aqu.}$ and $\gamma_{HD\text{-}Aqu.}$ of 22.5, 21.8 and 6.0 mN m^{-1}, respectively. The interfacial tension values of $\gamma_{PBzMA\text{-}HD}$ and $\gamma_{PBzMA\text{-}Aqu}$ were calculated using the OWRK method and the $\gamma_{DD\text{-}Aqu}$ as recorded in Figure 1d was used as a close estimate for $\gamma_{HD\text{-}Aqu.}$ Figure 3b shows that the predicted thermodynamic equilibrium morphology of PBzMA and HD is partial encapsulation. When the HD is evaporated under the extremely high vacuum during SEM imaging a dimple is left behind.

High magnification images of the particles in reactions MM1.25% and MM2.5% (Figure S4) appear to show a range of dimple ratios, even though the ratio of BzMA and HD should be equal in all particles. To investigate this further, for reaction MM1.25%, particles in SEM images that pointed directly upwards were sized. The particle and dimple radii were measured and the dimple volume (V) calculated geometrically (Figure 3c). The dimple volume was calculated as twice the volume of a spherical cap (Equation 4) where the cap base radius (a) was the radius of the dimple and the particle radius was r. The cap height (h) was calculated using equation 5.

$$V = 2\left[\frac{1}{3}\pi h^2(3r - h)\right] \quad (4)$$

$$R^2 = (R - h)^2 + a^2 \quad (5)$$

For 50 particles, the ratio of dimple/particle volume was calculated and plotted against particle diameter (Figure 3d). The experimental dimple/particle (HD/PBzMA+HD) volume ratio of 0.0775 has been added to the figure as the dotted line. With only 8 of 50 particles with 15% of the experimental ratio, the majority of sized particles have a much greater dimple volume than expected. There is also a general trend for the larger

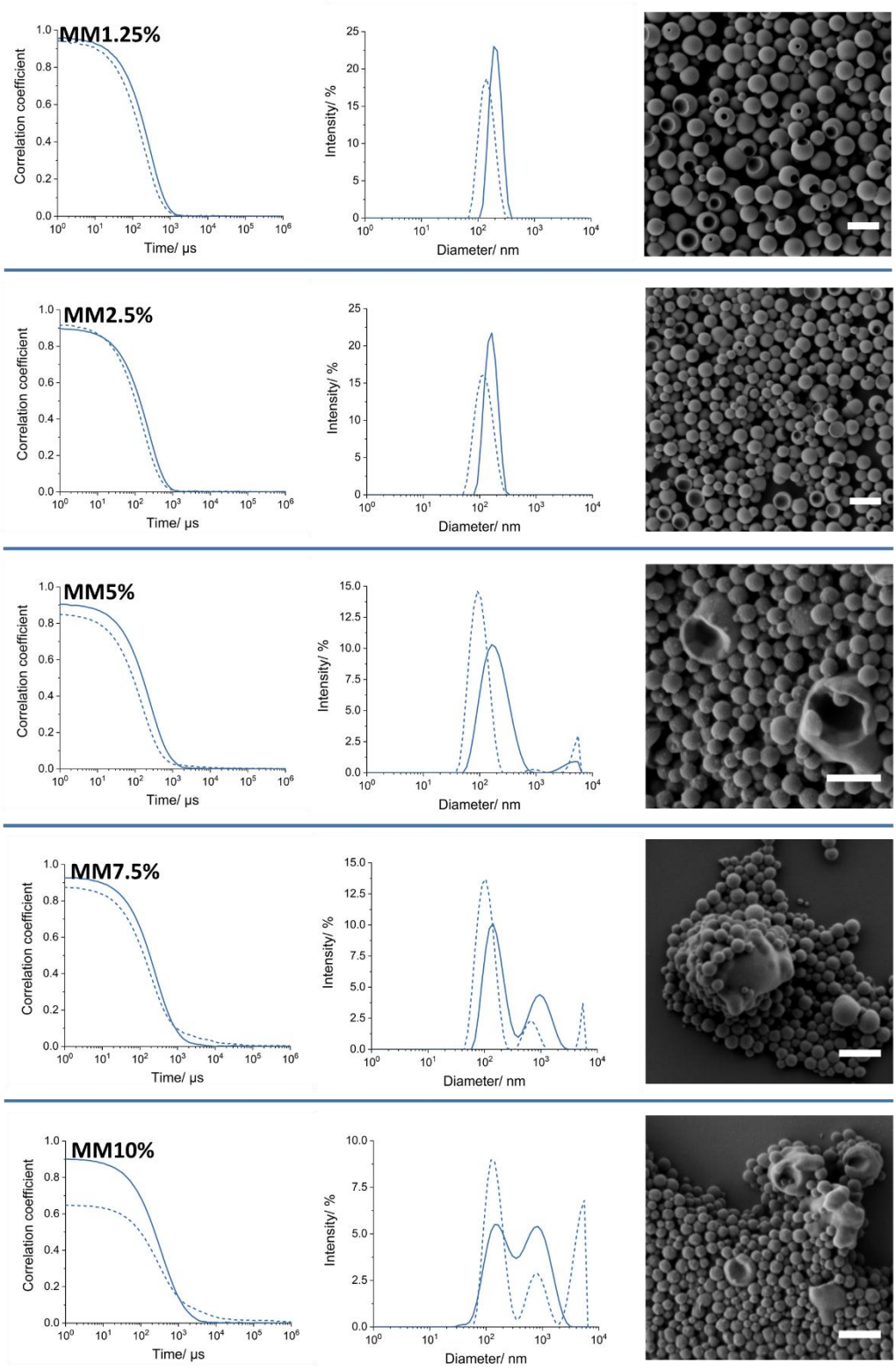

Figure 2 Left column) Correlograms of mini-emulsion monomer droplets and latex particles at full monomer conversion. **Middle column)** Intensity weighted size distributions of mini-emulsion monomer droplets and latex particles at full conversion. Droplet distributions are shown in dashed lines, particle distributions are shown as solid lines. **Right column)** Scanning electron micrographs of mini-emulsion poly(benzyl methacrylate) particles at full monomer conversion. Scale bars for all micrographs are 300 nm.

particles to have a greater ratio of dimple volume to total particle volume.

To explain this, we propose that an imbalance of HD and BzMA has to have occurred during polymerization. The HD acts as hydrophobe, preventing Ostwald ripening between monomer droplets before the reaction is initiated. However, once the reaction commences, the swelling power of particles can be increased through polymerization. This imbalance will trigger monomer transport. It is therefore possible that benzyl methacrylate could diffuse from one droplet/particle to

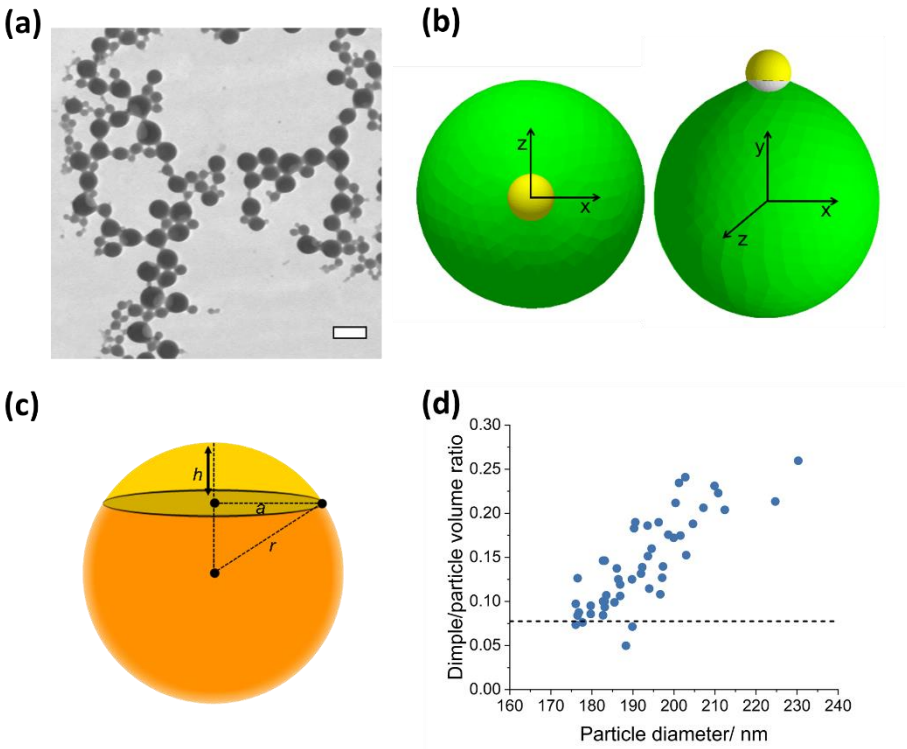

Figure 3 (a) TEM micrograph of dimpled particles from reaction MM1.25%, scale bar is 250 nm. (b) Predicted morphology of partially encapsulated hexadecane (yellow) by poly(benzyl methacrylate) (green). The left image shows the particle with the HD lobe pointing upwards. The right image is a vertical slice of the particle, showing the dimple/recess in grey. (c) Diagram showing the parameters used to determine the volume of a spherical cap. (d) Dimple/particle volume ratio plotted as a function of particle size for 50 particles imaged by SEM for reaction MM1.25%. Dimple volume was determined as two times the volume of a spherical cap with dimple radius *a*. Particle volume was determined from the radius *r*. Radii *a* and *r* were determined from SEM images using ImageJ software. The dotted line is the initial feed volume ratio of 0.0775.

another. However, since the water solubility of HD is much lower, loss of monomer from droplets increases the HD/BzMA volume ratio.

One potential underlying cause of monomer transport could be the presence of non-nucleated mini-emulsion droplets for a prolonged time. If the nucleation period was delayed due to slow radical production, there may be a mixture of growing particles and un-nucleated droplets, which would act as monomer reservoirs. However, the time taken for a single AIBN molecule to decompose in each droplet was calculated for reaction MM1.25% and found to be approximately 8 seconds. Although this calculation does not account for droplet size dispersity, nevertheless the nucleation time is fast and disproves the delayed nucleation theory.

Although droplet nucleation is fast, different rates of polymerization between individual particles may be the cause of the HD/BzMA imbalance. Smaller particles have a faster rate of polymerization due to a greater compartmentalization effect. During the reaction, monomer is stripped from the larger, and thus slower-growing particles, to the smaller ones. The irregularity of this process also explains how particles of the same diameter could have a wide difference in dimple/particle volume ratios (Figure 3d). This reason is plausible given the PDI measured by DLS is 0.154, indicating a broad distribution of droplet sizes. In addition, there also appears to be a smaller crop of particles in the TEM image of Figure 3(a). This suggests secondary nucleation and a new population of particles would also acts as a monomer sink. This secondary nucleation effect was also observed by Lu and co-workers using amphiphilic RAFT agents as stabilizers.[43–46] When synthesizing capsules of n-hexadecane or nonadecane, the group observed a secondary crop of solid particles if the water solubility of the RAFT stabilizer was too high. It is possible that the monomer used to grow these solid particles diffused from the original RAFT agent stabilized droplets.

The larger than expected dimples on particles in reactions MM1.25% and MM2.5% may also explain why the average particle size is higher than the droplet size (Figure 2, middle column). If the large hexadecane phase protrudes from the particles' surface the particles begin to resemble 'snowman' or dimer morphologies. The hydrodynamic radius of a dimer particle made from two identical spheres is predicted to increase by a factor of ≈1.39.[108–110] This factor overestimates the increase we observe but this is likely due to the smaller relative size of the HD and PBzMA spheres.

This effect of HD on DLS size was evidenced further by preparing an identical mini-emulsion to reaction MM1.25% but replacing HD with octadecyl methacrylate. After polymerization, no dimples were present (Figure S5), as expected, but there is now a near identical size distribution by DLS (Figure S6), with a slight decrease due to volume contraction on polymerization.

Mini-emulsion polymerization: multimodal distributions

Studying the DLS size distributions again (figure 2, middle column), in mini-emulsions stabilized by more than 2.5 wt% MM, both droplet and particles display bimodal or multimodal distributions. This issue also appears to worsen as the concentration of stabilizer increases, as is also apparent from the correlograms (figure 2, left column). To investigate this, the number average diameter as a function of weight percent macromonomer is plotted in Figure 4a. The number average droplet and particle size distributions for the five reactions are plotted in Figure S7. Increasing the amount of macromonomer from 1.25 to 5% w/w decreases the particle size, but at higher MM loadings the diameter plateaus. This plateau coincides with the onset of the multimodal distributions. The shift away from a monomodal particle distribution can be explained by considering the surface area a macromonomer occupies at the droplet/particle interface (a_{surf}) (Equation 6) Where N_{MM} and N_p are number of macromonomers and particles and r is particle radius.

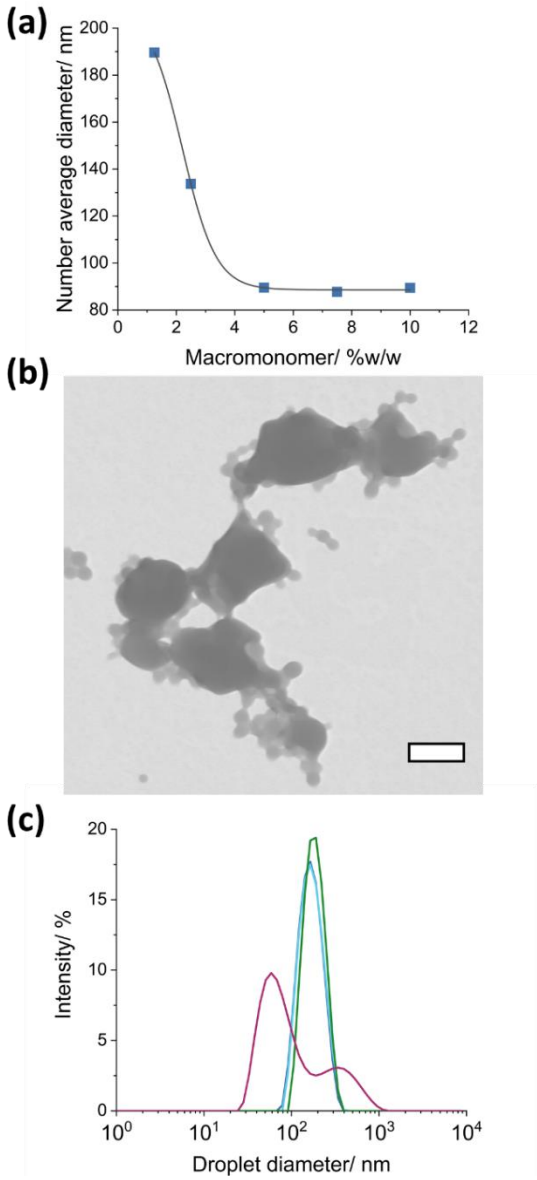

Figure 4 (**a**) Plot of number average diameter of poly(benzyl methacrylate) particles at full conversion as a function of macromonomer MM %w/w to dispersed phase. For samples with multimodal distribution (≥5% w/w MM) the number average diameter of the smallest population was recorded. The data has been fit with a Boltzmann function. **(b)** Transmission electron microscope image of MM7.5% showing large particles (250-600 nm diameter) and smaller particles (160 nm Z-avg. diameter), scale bar is 300 nm. **(c)** Droplet size distribution of mini-emulsions (MEs) measured by DLS. Size of starting ME using 2.5wt% MM (dark blue), ME after adding additional MM (light blue), ME after mixing with rotor stator homogenizer (green), ME after being processed with high pressure homogenizer.

$$a_{surf} = \frac{N_{MM}}{4\pi r^2 N_p} \quad (6)$$

Assuming all macromonomers in the system are at the particle interface, a_{surf} for reactions MM1.25% and MM2.5% is 41.3 nm^2 and 29.3 nm^2, respectively. Fitting the data with a Boltzmann sigmodal function allows us to estimate the lower limit of surface area MMs can occupy. The minima of the third derivative of the sigmodal function estimates full surface coverage will is reached for a particle 98.8 nm in diameter at 3.57 wt% MM. Using these theoretical values estimates the lower limit of a_{surf} to be 27.8 nm^2. At this area limit the geometrical constraints of the MM molecules prevent smaller droplets from forming and the interfacial tension of the droplets is not lowered any further. Any additional stabilizer added to the system will exist as excess in the aqueous phase. Since the CMC is low, this will be in the form of micelles.

Although an excess of macromonomers appears to be the cause of the larger particles, the mechanism of their formation is less clear. However, similar multimodal particle size distributions were reported by Hawkett and co-workers using macroRAFT stabilizer.[21] The authors stated the larger particles of the multimodal distribution were multi-hollow particles. Analysis of MM7.5% by transmission electron microscopy (Figure 4b) suggests that our large particles are also multi-hollow, and rupture under vacuum (Figure 2, MM5%). The reason for their formation may be due to depletion flocculation, as it is known that an excess of water-soluble polymer or micelles can trigger colloidal flocculation.[111,112] To investigate this further, a mini-emulsion was prepared using 2.5 wt% MM to dispersed phase. To this mini-emulsion, additional MM was added to total 10 wt% MM. The mini-emulsion was stirred for 60 mins before being homogenized with a rotor-stator mixer and finally homogenized by HPH. The droplet size distribution after each step is presented in Figure 4c and demonstrates that the formation of large droplets only occurs under high shear. We hypothesize that excess macromonomer stabilizer causes flocculation of monomer droplets directly after experiencing high shear forces. These forces, in our case, occur after the HPH homogenizing value but were also reported by Hawkett when using ultrasonication.[21]

Macromonomers as reactive stabilizers

Reactive surfactants are covalently bound to the particles they stabilize. This offers certain advantages over surface adsorbed stabilizers. On dilution or dialysis of a latex, surfactants will desorb from the particle surface to rebalance the aqueous phase concentration due to partitioning behaviour. This effect is stronger in small-molecule surfactants which generally

partition stronger towards the aqueous phase. To test stability of the macromonomer stabilized PBzMA particles, a portion of the latex from reaction MM2.5% was dialysed against deionized water (≥15 MΩ) for 21 days, sampling at 7 and 14 days. All of the samples were colloidally stable, the samples did not sediment or coagulate and size by DLS was unchanged from the original latex (figure S8, top). The zeta potential of the latex also remained stable between -54.2 and -54.8 mV (figure S8, bottom).

An advantage of polymeric surfactants over their low-molecular-weight counterparts is improved freeze-thaw stability. This characteristic describes the ability of the stabilizer to prevent coalescence of particles or droplets when the aqueous phase is frozen. Polymeric surfactants such as poly(ethylene glycol) methyl ether[113] or proteins such as sodium caseinate[114] show this behaviour due to formation of a dense stabilizer layer on the suspension. The effectiveness of the (P(BMA-*b*-[MAA-*co*-MMA]) macromonomers against freeze-thaw cycles was tested by cooling a PBzMA latex stabilised by 2.5 % w/w MM (reaction MM2.5%) to -18 °C for 24 hours before being warmed back to room temperature. Unfortunately, after thawing the latex, it was apparent that it had gelled due to excessive coagulation during freezing. It would appear that the hydrophilic (MAA-*co*-MMA) portion of the stabilizer does not offer enough static repulsion for latex stability under the compression of ice crystals. Despite this, it was possible to concentrate a latex by removal of water through evaporation. MM stabilised latexes could be concentrated to 42 % w/w solids whilst maintaining colloidal stability.

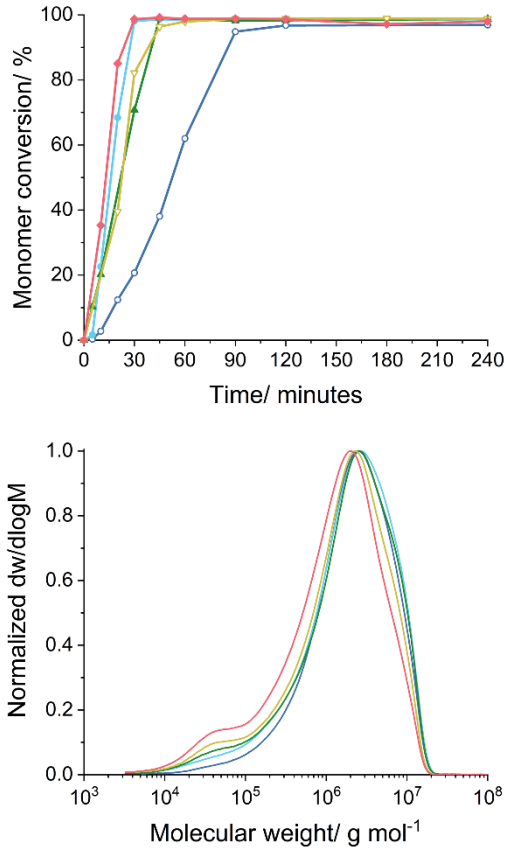

Figure 5 (Top) Cumulative monomer conversion as a function of time plotted for reactions using 1.25 (dark blue open circles), 2.5 (blue close circles), 5 (green closed triangles), 7.5 (yellow open triangles) and 10 (pink diamonds) wt% MM to dispersed phase. **(Bottom)** Molecular weight distributions of PBzMA latex taken after 120 minutes. Reactions using 1.25 (dark blue), 2.5 (light blue), 5 (green), 7.5 (yellow) and 10 (pink) wt% MM to dispersed phase are shown. All reactions at 120 minutes had reached ≥97 % conversion.

Due to the presence of the ω-unsaturated end group, it would be expected that the MM stabilizers may influence the rate of polymerization and PBzMA molecular weight through the same mechanisms as sulfur-based RAFT ME stabilizers. Monomer conversion as a function of time and final molecular weight distributions of the ME series are presented in Figure 5. All reactions with the exception of MM1.25% polymerized quickly and reached full conversion under 60 mins. The almost identical rate of polymerization for the reactions using 2.5 or 10 % w/w MM indicates there is little influence of the MM on rate. This in contrast to the observed retardation of rate in ab initio RAFT emulsion polymerization.[115–117] The slightly slower rates of reactions using 5 and 7.5 % w/w MM can be attributed to experimental variation. The exception to this observation is the reaction using the lowest amount of MM (MM1.25%) and is related to particle size. With a number average diameter of 180 nm, reaction MM1.25% has the largest average size in the series and thus the lowest number of particles (N_p). As the rate of polymerization has a positive relationship to N_p, it is to be expected that MM1.25% will react the slowest (figure 4a).

For ME polymerizations using of thiocarbonylthio-based RAFT agents, over the duration of the reaction molecular weight generally follows theorical values.[21,42,44,46,47,118,119] The predicted number average molecular weight of the MM series ranges from 70 to 140 kg.mol^{-1}. From data in figure 5 (full spectra Figure S9), although the MM does have minor effect on the molecular weight distribution, the experimental molecular weight greatly exceeds the predicted value. This limited effect on molecular weight by the MM is due to their low chain transfer constant ($C_s = k_{tr}/k_p$), estimated to be around 0.2-0.4.[40] Due to a high local monomer concentration in the mini-emulsion droplets, control of monomer propagation typical in RDRP reactions, is absent up to high monomer conversion levels.

The final point to consider is the degree of MM consumption during the reactions. In the molecular weight distributions (figure 5), a lower molecular weight peak/shoulder at 40 kg mol^{-1} is present. This is attributed to residual MM and becomes more pronounced at higher loadings. Some of this excess may be unreacted MM that were not at the locus of polymerization. From the difference in molecular weight distributions, we know some MM has taken part in the reaction but exactly how much? The answer to this question and the limitations of SF-RAFT (mini)emulsion polymerization will be explored in a future kinetic study.

Conclusions

The physical and thermodynamic characteristics of the poly(*n*-butyl methacrylate-*block*-[methacrylic acid-*co*-methyl methacrylate]) macromonomer micelles were studied. The low CMC was comparable to other polymeric stabilisers. The micelle

size measured by SAXS was lower than the value obtained by DLS. This was due to a combination of low scattering intensity of the corona block in SAXS and the high molecular weight protruding chains from the outer regions of the micelles into the water phase in DLS. The dynamics of the *n*-dodecane-water interfacial tension in the presence of MM was found to be slow. This was a result of the low CMC and high degree of MAA ionization. Nevertheless, under high-shear during mechanical stirring and homogenization these dynamics were not relevant and the MM stabilizers were able to stabilize PBzMA mini-emulsion droplets and the resulting latexes made at 20 % w/w solid contents.

It was observed that particles stabilized with 1.25 and 2.5 wt% MM were bowl-shaped. The bowls were a result of the phase separation of hexadecane from PBzMA during polymerization, as predicted by a thermodynamic model. Furthermore, the radius or volume of the dimple left by the evaporated HD was greater than expected for the larger particles, with respect to overall particle size/volume. We theorise that this is caused by the transfer of monomer throughout polymerization from the larger particles to the smaller ones, as the latter polymerized faster as a result of compartmentalization.

Particles stabilised with ≥5 wt% MM showed bimodal droplet and particle distributions. It was found that larger population of particle originated as droplets formed during homogenization in the presence of excess MM.

Lastly, the effectiveness of the reactive stabilisers was tested in terms of particle stability and molecular weight control. Unfortunately, the macromonomers were not able to protect the particles against coalescence when the latex was frozen. However, they offered robust stability against prolonged dialysis and latex concentration upon water removal. SEC analyses of the five reactions showed a slight impact of the MMs but very high molecular weight polymer was produced in all cases. Residual MM at the end of the reactions suggests it was not all incorporated.

Author Contributions

Joshua R. Booth: Conceptualization, formal analysis, investigation, methodology, project administration, resources validation, visualization, writing – original draft. **Joshua D. Davies:** Formal analysis, investigation, resources, software, validation, visualization, writing – review & editing. **Stefan A. F. Bon:** Conceptualization, supervision, project administration, methodology, formal analysis, resources, funding acquisition, writing – review and editing.

Conflicts of interest

There are no conflicts to declare.

Acknowledgements

The authors would like to thank the University of Warwick Polymer Characterization Research Technology Platform (RTP), specifically Dr Daniel Lester and Dr Rachel Hand, for maintenance and access to GPC and GC equipment. The authors give thanks to Dr Steven Huband, University of Warwick for carrying out small angle x-ray scattering measurements and data processing. The authors would also like to thank the University of Warwick electron microscopy RTP for the use of EM equipment and providing specialist training.

References

1 I. Piirma, *Makromolekulare Chemie. Macromolecular Symposia*, 1990, **35–36**, 467–475.
2 G. Riess and C. Labbe, *Macromolecular Rapid Communications*, 2004, **25**, 401–435.
3 H. Cramail, E. Cloutet and K. Radhakrishnan, in *Macromolecular Engineering: Precise Synthesis, Materials Properties, Applications*, John Wiley & Sons, Ltd, 2011, pp. 2181–2223.
4 P. Raffa, D. A. Z. Wever, F. Picchioni and A. A. Broekhuis, *Chem. Rev.*, 2015, **115**, 8504–8563.
5 A. Durand and E. Marie, *Advances in Colloid and Interface Science*, 2009, **150**, 90–105.
6 J. Ugelstad, M. S. El-Aasser and J. W. Vanderhoff, *Journal of Polymer Science: Polymer Letters Edition*, 1973, **11**, 503–513.
7 K. Landfester, *Macromolecular Rapid Communications*, 2001, **22**, 896–936.
8 K. Landfester, R. Rothe and M. Antonietti, *Macromolecules*, 2002, **35**, 1658–1662.
9 B. Erdem, E. D. Sudol, V. L. Dimonie and M. S. El-Aasser, *Macromolecular Symposia*, 2000, **155**, 181–198.
10 N. Bechthold, F. Tiarks, M. Willert, K. Landfester and M. Antonietti, *Macromolecular Symposia*, 2000, **151**, 549–555.
11 D. Hoffmann, K. Landfester and M. Antonietti, *Magnetohydrodynamics*, 2001, **37**, 217–221.
12 F. Tiarks, K. Landfester and M. Antonietti, *Langmuir*, 2001, **17**, 908–918.
13 A. J. P. van Zyl, D. de Wet-Roos, R. D. Sanderson and B. Klumperman, *European Polymer Journal*, 2004, **40**, 2717–2725.
14 K. Landfester, N. Bechthold, F. Tiarks and M. Antonietti, *Macromolecules*, 1999, **32**, 5222–5228.
15 W. Ostwald, *Lehrbuch der allgemeinen chemie*, Leipzig, W. Engelmann, 1885.
16 A. J. Ardell, *Acta Metallurgica*, 1972, **20**, 61–71.
17 W. I. Higuchi and J. Misra, *Journal of Pharmaceutical Sciences*, 1962, **51**, 459–466.
18 L. L. Hecht, C. Wagner, K. Landfester and H. P. Schuchmann, *Langmuir*, 2011, **27**, 2279–2285.
19 G. Baskar, K. Landfester and M. Antonietti, *Macromolecules*, 2000, **33**, 9228–9232.
20 M. Manguian, M. Save, C. Chassenieux and B. Charleux, *Colloid and Polymer Science*, 2005, **284**, 142–150.

21 B. T. T. Pham, H. Zondanos, C. H. Such, G. G. Warr and B. S. Hawkett, *Macromolecules*, 2010, **43**, 7950–7957.
22 D. Crespy, A. Musyanovych and K. Landfester, *Colloid Polym Sci*, 2006, **284**, 780–787.
23 M. Amaral and J. M. Asua, *Macromolecular Rapid Communications*, 2004, **25**, 1883–1888.
24 M. Amaral, H. de Brouwer, S. V. Es and J. M. Asua, *Macromolecular Symposia*, 2005, **226**, 167–176.
25 C. Lefay, M. Save, B. Charleux, S. Magnet, C. Lefay, M. Save, B. Charleux and S. Magnet, *Australian Journal of Chemistry*, 2006, **59**, 544–548.
26 S. Wang, X. Wang and Z. Zhang, *European Polymer Journal*, 2007, **43**, 178–184.
27 A. N. F. Peck and J. M. Asua, *Macromolecules*, 2008, **41**, 7928–7932.
28 M.-S. Lim and H. Chen, *Journal of Polymer Science Part A: Polymer Chemistry*, 2000, **38**, 1818–1827.
29 L. Houillot, J. Nicolas, M. Save, B. Charleux, Y. Li and S. P. Armes, *Langmuir*, 2005, **21**, 6726–6733.
30 S. Wang and F. J. Schork, *Journal of Applied Polymer Science*, 1994, **54**, 2157–2164.
31 N. Kim, E. D. Sudol, V. L. Dimonie and M. S. El-Aasser, *Macromolecules*, 2003, **36**, 5573–5579.
32 J.-W. Kim, J.-Y. Ko and K.-D. Suh, *Macromolecular Rapid Communications*, 2001, **22**, 257–261.
33 J.-W. Kim, J.-Y. Ko, J.-G. Park, J.-B. Jun, I.-S. Chang and K.-D. Suh, *Journal of Applied Polymer Science*, 2002, **85**, 328–332.
34 A. Guyot and K. Tauer, in *Polymer Synthesis*, Springer, Berlin, Heidelberg, 1994, pp. 43–65.
35 T. P. Le, G. Moad, E. Rizzardo, S. H. Thang, WO pat., WO1998001478A1, 1998.
36 J. Chiefari, Y. K. (Bill) Chong, F. Ercole, J. Krstina, J. Jeffery, T. P. T. Le, R. T. A. Mayadunne, G. F. Meijs, C. L. Moad, G. Moad, E. Rizzardo and S. H. Thang, *Macromolecules*, 1998, **31**, 5559–5562.
37 P. Corpart, D. Charmot, S. Z. Zard, T. Biadatti, D. Michelet, US Pat., US6153705A, 2000.
38 J. Krstina, C. L. Moad, G. Moad, E. Rizzardo, C. T. Berge and M. Fryd, *Macromolecular Symposia*, 1996, **111**, 13–23.
39 J. Krstina, G. Moad, E. Rizzardo, C. L. Winzor, C. T. Berge and M. Fryd, *Macromolecules*, 1995, **28**, 5381–5385.
40 C. L. Moad, G. Moad, E. Rizzardo and S. H. Thang, *Macromolecules*, 1996, **29**, 7717–7726.
41 D. J. Keddie, G. Moad, E. Rizzardo and S. H. Thang, *Macromolecules*, 2012, **45**, 5321–5342.
42 B. T. T. Pham, D. Nguyen, C. J. Ferguson, B. S. Hawkett, A. K. Serelis and C. H. Such, *Macromolecules*, 2003, **36**, 8907–8909.
43 Y. Luo and H. Gu, *Macromolecular Rapid Communications*, 2006, **27**, 21–25.
44 Y. Luo and H. Gu, *Polymer*, 2007, **48**, 3262–3272.
45 F. Lu, Y. Luo and B. Li, *Macromolecular Rapid Communications*, 2007, **28**, 868–874.
46 F. Lu, Y. Luo and B. Li, *Industrial & Engineering Chemistry Research*, 2010, **49**, 2206–2212.
47 T. Boursier, I. Chaduc, J. Rieger, F. D'Agosto, M. Lansalot and B. Charleux, *Polymer Chemistry*, 2011, **2**, 355–362.
48 Y. Li, L. Christian-Tabak, V. L. F. Fuan, J. Zou and C. Cheng, *Journal of Polymer Science Part A: Polymer Chemistry*, 2014, **52**, 3250–3259.
49 C. Grazon, J. Rieger, P. Beaunier, R. Méallet-Renault and G. Clavier, *Polym. Chem.*, 2016, **7**, 4272–4283.
50 A. A. Gridnev and S. D. Ittel, *Chem. Rev.*, 2001, **101**, 3611–3660.
51 I. Schreur-Piet and J. P. A. Heuts, *Polymer Chemistry*, 2017, **8**, 6654–6664.
52 A. Marathianos, A. M. Wemyss, E. Liarou, J. R. Jones, A. Shegiwal, J. S. Town, D. W. Lester, Y. Li and D. M. Haddleton, *ACS Appl. Polym. Mater.*, 2021, **3**, 3185–3196.
53 D. Zhou, R. P. Kuchel and P. B. Zetterlund, *Polymer Chemistry*, 2017, **8**, 4177–4181.
54 A. Lotierzo, R. M. Schofield and S. A. F. Bon, *ACS Macro Letters*, 2017, **6**, 1438–1443.
55 L. Chen, L. Yan, Q. Li, C. Wang and S. Chen, *Langmuir*, 2010, **26**, 1724–1733.
56 I. Schreur-Piet, A. M. Van Herk, J. Laven and J. P. A. Heuts, *Industrial and Engineering Chemistry Research*, 2019, **58**, 21105–21117.
57 I. Schreur-Piet and J. P. A. Heuts, *ACS Appl. Polym. Mater.*, 2021, **3**, 4616–4624.
58 W. Yang and R. A. Hutchinson, *Macromolecular Reaction Engineering*, 2016, **10**, 71–81.
59 M. Zhang and R. A. Hutchinson, *Macromolecules*, 2018, **51**, 6267–6275.
60 W. H. Lee, J. R. Booth and S. A. F. Bon, *Biomacromolecules*, 2020, **21**, 4599–4614.
61 A. Shegiwal, A. M. Wemyss, E. Liarou, J. Town, G. Patias, C. J. Atkins, A. Marathianos, D. W. Lester, S. Efstathiou and D. M. Haddleton, *European Polymer Journal*, 2020, **125**, 109491.
62 A. Lotierzo, B. W. Longbottom, W. H. Lee and S. A. F. Bon, *ACS Nano*, 2019, **13**, 399–407.
63 A. Lotierzo, S. P. Meaney and S. A. F. Bon, *Polymer Chemistry*, 2019, **10**, 6600–6608.
64 V. E. Trommsdorff, H. Köhle and P. Lagally, *Die Makromolekulare Chemie*, 1948, **1**, 169–198.
65 R. G. W. Norrish and R. R. Smith, *Nature*, 1942, **150**, 336–337.
66 A. Bakac, M. E. Brynildson and J. H. Espenson, *Inorganic Chemistry*, 1986, **25**, 4108–4114.
67 K. G. Suddaby, D. M. Haddleton, J. J. Hastings, S. N. Richards and J. P. O'Donnell, *Macromolecules*, 1996, **29**, 8083–8091.
68 I. Lacík, M. Stach, P. Kasák, V. Semak, L. Uhelská, A. Chovancová, G. Reinhold, P. Kilz, G. Delaittre, B. Charleux, I. Chaduc, F. D'Agosto, M. Lansalot, M. Gaborieau, P. Castignolles, R. G. Gilbert, Z. Szablan, C. Barner-Kowollik, P. Hesse and M. Buback, *Macromolecular Chemistry and Physics*, 2015, **216**, 23–37.
69 E. Kühnel, D. D. P. Laffan, G. C. Lloyd-Jones, T. Martínez del Campo, I. R. Shepperson and J. L. Slaughter, *Angewandte Chemie International Edition*, 2007, **46**, 7075–7078.
70 A. Rudin and H. L. W. Hoegy, *Journal of Polymer Science Part A-1: Polymer Chemistry*, 1972, **10**, 217–235.
71 M. D. Zammit, M. L. Coote, T. P. Davis and G. D. Willett, *Macromolecules*, 1998, **31**, 955–963.

72 A. Katchalsky and P. Spitnik, *Journal of Polymer Science*, 1947, **2**, 432–446.
73 S. Kawaguchi, A. Yekta and M. A. Winnik, *Journal of Colloid and Interface Science*, 1995, **176**, 362–369.
74 P. Ravi, C. Wang, K. C. Tam and L. H. Gan, *Macromolecules*, 2003, **36**, 173–179.
75 E. Lejeune, M. Drechsler, J. Jestin, A. H. E. Müller, C. Chassenieux and O. Colombani, *Macromolecules*, 2010, **43**, 2667–2671.
76 E. Lejeune, C. Chassenieux and O. Colombani, in *Trends in Colloid and Interface Science XXIV*, eds. V. Starov and K. Procházka, Springer, Berlin, Heidelberg, 2011, pp. 7–16.
77 J. N. Israelachvili, D. J. Mitchell and B. W. Ninham, *J. Chem. Soc., Faraday Trans. 2*, 1976, **72**, 1525–1568.
78 F. Li, M. Schellekens, J. de Bont, R. Peters, A. Overbeek, F. A. M. Leermakers and R. Tuinier, *Macromolecules*, 2015, **48**, 1194–1203.
79 G. Moad and D. H. Solomon, *The Chemistry of Radical Polymerization*, Elsevier, 2nd edn., 2005.
80 T. Liu, H. Schuch, M. Gerst and B. Chu, *Macromolecules*, 1999, **32**, 6031–6042.
81 D. E. Ganeva, E. Sprong, H. de Bruyn, G. G. Warr, C. H. Such and B. S. Hawkett, *Macromolecules*, 2007, **40**, 6181–6189.
82 M. Rubinstein, *Polymer Physics*, Oxford University Press, 2003.
83 P. J. Flory, *Statistical Mechanics of Chain Molecules*, Hanser Publishers, 1989.
84 Z. Xu, N. Hadjichristidis and L. J. Fetters, *Macromolecules*, 1984, **17**, 2303–2306.
85 J. Brandrup, E. H. Immergut and E. A. Grulke, *Polymer Handbook*, Wiley, 2003.
86 P. S. Mohanty, H. Dietsch, L. Rubatat, A. Stradner, K. Matsumoto, H. Matsuoka and P. Schurtenberger, *Langmuir*, 2009, **25**, 1940–1948.
87 M. Jacquin, P. Muller, R. Talingting-Pabalan, H. Cottet, J. F. Berret, T. Futterer and O. Théodoly, *Journal of Colloid and Interface Science*, 2007, **316**, 897–911.
88 S. George, R. Champagne-Hartley, G. Deeter, D. Campbell, B. Reck, D. Urban and M. Cunningham, *Macromolecules*, 2015, **48**, 8913–8920.
89 S. R. George, R. Champagne-Hartley, G. A. Deeter, J. D. Campbell, B. Reck, D. Urban and M. F. Cunningham, *Macromolecules*, 2017, **50**, 315–323.
90 A. Guinier and G. Fournet, *Small-angle scattering of X-rays*, Wiley, New York, 1955.
91 J. B. Hayter and J. Penfold, *Molecular Physics*, 1981, **42**, 109–118.
92 J.-P. Hansen and J. B. Hayter, *Molecular Physics*, 1982, **46**, 651–656.
93 S. Zeppieri, J. Rodríguez and A. L. López de Ramos, *J. Chem. Eng. Data*, 2001, **46**, 1086–1088.
94 R. Aveyard and B. J. Briscoe, *Trans. Faraday Soc.*, 1970, **66**, 2911–2916.
95 R. Aveyard and S. M. Saleem, *J. Chem. Soc., Faraday Trans. 1*, 1976, **72**, 1609–1617.
96 Xi Yuan Hua and M. J. Rosen, *Journal of Colloid and Interface Science*, 1988, **124**, 652–659.
97 O. Théodoly, M. Jacquin, P. Muller and S. Chhun, *Langmuir*, 2009, **25**, 781–793.
98 F. Millet, P. Perrin, M. Merlange and J.-J. Benattar, *Langmuir*, 2002, **18**, 8824–8828.
99 R. Roe, *J. Chem. Phys.*, 1974, **60**, 4192–4207.
100 M. A. C. Stuart, J. M. H. M. Scheutjens and G. J. Fleer, *Journal of Polymer Science: Polymer Physics Edition*, 1980, **18**, 559–573.
101 G. G. Stokes, in *Transactions of the Cambridge Philosophical Society*, University Press, Cambridge, 1856.
102 M. Y. Koroleva and E. V. Yurtov, *Russian Chemical Reviews*, 2012, **81**, 21–43.
103 M. Manea, A. Chemtob, M. Paulis, J. C. de la Cal, M. J. Barandiaran and J. M. Asua, *AIChE Journal*, 2008, **54**, 289–297.
104 S. Torza and S. G. Mason, *Science*, 1969, **163**, 813–814.
105 A. J. P. van Zyl, R. D. Sanderson, D. de Wet-Roos and B. Klumperman, *Macromolecules*, 2003, **36**, 8621–8629.
106 J. Berthier and K. Brakke, *The Physics of Microdroplets*, Wiley-Scrivener, 2012.
107 The Physics of Microdroplets - Chapter 9, http://facstaff.susqu.edu/brakke/aux/physicsofmicrodroplets/chap9/chap9.html, (accessed 19 October 2021).
108 J. Happel and H. Brenner, *Low Reynolds number hydrodynamics: with special applications to particulate media*, Springer Science & Business Media, 2012.
109 W. L. Yu, E. Matijević and M. Borkovec, *Langmuir*, 2002, **18**, 7853–7860.
110 W. L. Yu and M. Borkovec, *J. Phys. Chem. B*, 2002, **106**, 13106–13110.
111 R. M. Fitch, *Polymer Colloids*, 3Island Press, 1971.
112 T. A. Adamson, A. W. Adamson and A. P. Gast, *Physical Chemistry of Surfaces*, Wiley, 1997.
113 R. H. Ottewill, R. Satgurunathan, F. A. Waite and M. J. Westby, *British Polymer Journal*, 1987, **19**, 435–440.
114 J. Palanuwech and J. N. Coupland, *Colloids and Surfaces A: Physicochemical and Engineering Aspects*, 2003, **223**, 251–262.
115 G. Moad, J. Chiefari, Y. K. (Bill) Chong, J. Krstina, R. T. A. Mayadunne, A. Postma, E. Rizzardo and S. H. Thang, *Polymer International*, 2000, **49**, 993–1001.
116 M. J. Monteiro, M. Hodgson and H. De Brouwer, *Journal of Polymer Science Part A: Polymer Chemistry*, 2000, **38**, 3864–3874.
117 W. Smulders, R. G. Gilbert and M. J. Monteiro, *Macromolecules*, 2003, **36**, 4309–4318.
118 D. Nguyen, H. S. Zondanos, J. M. Farrugia, A. K. Serelis, C. H. Such and B. S. Hawkett, *Langmuir*, 2008, **24**, 2140–2150.
119 L. Yang, J. Yin, Q. Zhao, Z. Cui, Y. Shen and Y. Wang, *Colloid Polym Sci*, 2018, **296**, 1615–1625.

